Cardiac Neurotransmission Imaging*

Ignasi Carrió

Department of Nuclear Medicine, Hospital Sant Pau, Barcelona, Spain

Cardiac neurotransmission imaging with SPECT and PET allows in vivo assessment of presynaptic reuptake and neurotransmitter storage as well as of regional distribution and activity of postsynaptic receptors. In this way, the biochemical processes that occur during neurotransmission can be investigated in vivo at a micromolar level using radiolabeled neurotransmitters and receptor ligands. SPECT and PET of cardiac neurotransmission characterize myocardial neuronal function in primary cardioneuropathies, in which the heart has no significant structural abnormality, and in secondary cardioneuropathies caused by the metabolic and functional changes that take place in different diseases of the heart. In patients with heart failure, the assessment of sympathetic activity has important prognostic implications and will result in better therapy and outcome. In diabetic patients, scintigraphic techniques allow the detection of autonomic neuropathy in early stages of the disease. In conditions with a risk of sudden death, such as idiopathic ventricular tachycardia and arrhythmogenic right ventricular cardiomyopathy, PET and SPECT reveal altered neuronal function when no other structural abnormality is seen. In patients with ischemic heart disease, heart transplantation, drug-induced cardiotoxicity, and dysautonomias, assessment of neuronal function can help characterize the disease and improve prognostic stratification. Future directions include the development of tracers for new types of receptors, the targeting of second messenger molecules, and the early assessment of cardiac neurotransmission in genetically predisposed subjects for prevention and early treatment of heart failure.

Key Words: cardiac neurotransmission; cardiac PET; cardiac SPECT; cardiomyopathies

J Nucl Med 2001; 42:1062–1076

Visualization and quantitation with SPECT and PET of the pathophysiologic processes that take place in the nerve terminals, synaptic clefts, and postsynaptic sites in the heart can be referred to as cardiac neurotransmission imaging (Fig. 1). Clearly, the nerves are as important as the coronary arteries for many of the functions of the heart, particularly cardiac rhythm, conduction, and repolarization (*1*). In many clinical circumstances, these processes appear altered although no structural heart disease can be shown by traditional morphologic and functional investigations. In such a situation, evaluation of abnormalities of the cardiac nerves, cardiac ganglia, and neurotransmission process may be clinically relevant. In the United States, approximately 300,000 sudden cardiac deaths occur each year, and almost 20% of them are in patients without evidence of coronary artery disease (*2*). Nuclear medicine is currently the only imaging modality with sufficient sensitivity to offer in vivo visualization of cardiac neurotransmission at a micromolar level. Such a unique capability has great diagnostic potential and currently allows noninvasive classification of dysautonomias, characterization of pathologic myocardial substrate in arrhythmogenic cardiomyopathies, and assessment of neuronal status in coronary artery disease. This article will discuss the pathophysiologic basis of cardiac neurotransmission and will focus on the main clinical applications, from those for which only preliminary but compelling data are available to those that are well established.

Received Dec. 8, 2000; revision accepted Mar. 9, 2001.

For correspondence or reprints contact: Ignasi Carrió, MD, Hospital Sant Pau, Pare Claret 167, 08025-Barcelona, Spain.

*NOTE: FOR CE CREDIT, YOU CAN ACCESS THIS ACTIVITY THROUGH THE SNM WEB SITE (http://www.snm.org/education/ce_online.html) UNTIL JULY 2002.

CARDIAC INNERVATION AND NEUROTRANSMISSION

The autonomic nervous system is divided into the sympathetic and parasympathetic subsystems (*3*,*4*). The autonomic outflow is controlled by regulatory centers in the midbrain, hypothalamus, pons, and medulla. These regulatory centers integrate input signals coming from other areas of the brain as well as afferent stimuli coming from baroreceptors and chemoreceptors distributed in the skin, muscles, and viscera. Subsequently, efferent signals follow descending pathways in the lateral funiculus of the spinal cord that terminate on cell bodies placed in the intermediolateral and intermediomedial columns. The major neurotransmitters of the sympathetic and parasympathetic systems are norepinephrine and acetylcholine, which define the stimulatory and inhibitory physiologic effects of each system. Sympathetic fibers leave the spinal cord at segments T1 to L2–3. Preganglionic sympathetic fibers consist of small myelinated fibers that come off the spinal roots as white rami communicantes and synapse in the paravertebral ganglia. Gray rami communicantes that rejoin the anterior spinal roots and connect with body organs are formed by small unmyelinated postganglionic fibers (*5*). Adrenergic fibers that innervate the heart originate in the left and right stellate ganglia. The left stellate innervates the right ventricle, whereas the right stellate innervates the anterior and lateral

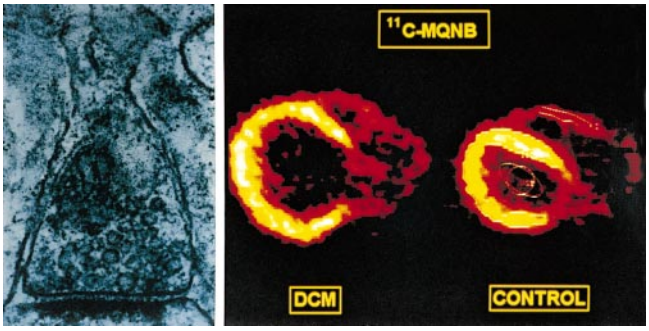

FIGURE 1. Concept of cardiac neurotransmission imaging. On left, electron microscopy of cardiac synapse shows postsynaptic concentration of neurotransmitter. On right, methylquinuclidinyl benzylate (MQNB) and PET show in vivo visualization of cardiac muscarinic receptors in patient with dilated cardiomyopathy (DCM) and in healthy volunteer (CONTROL).

portions of the heart. The adrenergic fibers travel the subendocardium, following the coronary vessels from the base to the apex of the heart (*6*). The parasympathetic innervation of the heart is scarce in comparison; the inferior wall is the region with a higher density of parasympathetic fibers. Parasympathetic innervation originates from the medulla and follows through the right and left vagus nerves, which then divide into the superior and inferior cardiac nerves. Parasympathetic fibers modulate sinoatrial nodal and atrioventricular nodal function and innervate the atria, whereas vagal fibers to the ventricles are sparse.

Activation of the sympathetic branch of the autonomic nervous system or a rise in the level of catecholamines may result in cardiac adrenergic stimulation and in subsequent changes in the contractile and electrophysiologic status of the heart. The sympathetic nervous system is a vasoactive neurohormonal system that evolved as a primary means of preserving circulatory homeostasis during environmental stress. Increased sympathetic activity, with respect to the cardiovascular system, leads to peripheral vasoconstriction, sodium and water retention, and the activation of other neurohormonal systems. At a cardiac level, sympathetic activation results in an increased heart rate (chronotropic effect), augmented contractility (inotropic effect), and enhanced atrioventricular conduction (dromotropic effect). In the heart, an increased presynaptic neuronal release of norepinephrine is thought to be accompanied by an impaired neuronal uptake of noradrenaline by the sympathetic nerve endings and by a reduced number of uptake sites. These neuronal alterations will increase the norepinephrine concentration in the synaptic cleft.

The source of synthesis of norepinephrine is the amino acid tyrosine, which is converted to dihydroxyphenylalanine and then to dopamine. Dopamine is transported into storage vesicles by active transport and transformed to norepinephrine by the enzyme β-hydroxylase. The action of norepinephrine in the synaptic cleft is terminated mainly by reuptake into the presynaptic nerve ending by the uptake-1 carrier. Other related amines such as epinephrine and guanethidine are also transported by uptake-1, which can be inhibited by cocaine and desipramine. A quantitatively less significant transport protein, uptake-2, removes norepinephrine from the extracellular space. Free cytosolic norepinephrine is degraded rapidly to dihydroxyphenylglycol by monoamine oxidase and passes through the presynaptic cell membrane into the extracellular space by passive diffusion.

Adrenergic neurotransmitters bind to the postsynaptic β-adrenoceptors. β_1- and β_2-receptors are located in the sarcolemma of the myocytes with a proportion of 80%:20%. This distribution may vary in the failing human heart, with a higher proportion of β_2-receptors being expressed (*7*). β_1-receptors are occupied by norepinephrine, whereas β_2-receptors are occupied by epinephrine. β_1-receptors are located mainly in the synaptic cleft, whereas β_2-receptors are located far from the synaptic cleft to protect epinephrine arriving as a hormone or from extracardiac neuronal production from neuronal reuptake. β-adrenoceptors are coupled to G protein subunits, and stimulation of β-adrenoceptors results in increased adenylyl cyclase activity, subsequently leading to intracellular cyclic adenosine monophosphate (cAMP) formation and phosphorylation of intracellular proteins, mediated by protein kinases, and influencing calcium transients and repolarization. When prolonged excessive stimulation of adrenergic receptors takes place, the first consequence is desensitization of adrenoceptors, followed by downregulation with enhanced receptor degradation and decreased receptor synthesis (*7,8*). The next step is uncoupling of the receptors with overexpression of inhibitory G proteins and β-ARK and downregulation of adenylyl cyclase. The final clinical consequence is decreased myocardial reserve and impaired exercise capacity.

On the other hand, parasympathetic innervation is distributed throughout the atrial and ventricular walls, with a gradient from the former to the latter, with acetylcholine being the main neurotransmitter. Acetylcholine is synthesized by transport of choline into the cytosol of the nerve terminal through the high-affinity choline transporter and acetylation by choline acetyltransferase. The transmitter is then stored in vesicles and released when nerve stimulation activates muscarinic receptors. The effects are terminated by rapid degradation by acetylcholinesterase. Muscarinic cholinergic receptors play a role in the regulation of heart rate and contractile function in balance with adrenergic receptors. The main mechanism of action seems to be inhibition of the guanosine triphosphate (GTP)-activated adenylate cyclase activity mediated by a GTP-binding α-regulatory protein (G_i). G_i inactivates the catalytic subunit of adenylate cyclase, thereby reducing intracellular cAMP levels and exerting an antiadrenergic effect. Therefore, the parasympathetic system acts through muscarinic cholinergic inhibition of β-adrenergic cardiac responsiveness. In this way, adrenaline is enhanced and inotropic stimulation is induced by noradrenaline after parasympathetic blockade with atropine.

Cardiac function declines with age. This is a physiologic multifactorial process in which a decrease in cardiac responsiveness to β-adrenergic stimulation is one of the most prominent alterations. Several possible defects can account for this age-dependant reduced responsiveness: for example, reduction in the number of β-adrenergic receptors because of increased sympathetic activity with aging and subsequent receptor downregulation, and changes in the functional state of the receptors with functional deficits of G-protein–coupled proteins or post-cAMP defects.

IN VIVO METHODS TO ASSESS SYMPATHETIC ACTIVITY IN HUMANS

Sympathetic Nervous System at a Presynaptic Level

The sympathetic neuronal firing rate can be assessed directly by means of microneurography. However, microneurography has significant limitations because it can be applied only to the nerves of skin and muscles and not to the nerves of internal organs such as the heart. In heart failure, for example, systemic sympathetic activity may be normal whereas sympathetic activity at a cardiac level is increased.

In myocardial tissue obtained by endomyocardial biopsy, noradrenaline concentrations and the cardiac noradrenaline uptake sites can be quantified in vitro. In addition, cardiac noradrenaline kinetics can be assessed biochemically in vivo. Cardiac neuronal uptake, which is the most important mechanism for the inactivation of noradrenaline, can be assessed in vivo by 3 techniques. The first is by determining the cardiac removal of intravenously infused radioactive noradrenaline before and after neuronal uptake blockade with desipramine. The second is by measuring the difference between the fractional extraction of radioactive noradrenaline and radioactive isoproterenol, which is not a substrate for neuronal uptake. The third is by measuring regional arteriovenous differences of radioactive and endogenous dihydroxyphenylglycol, which is an exclusively intraneuronal metabolite of noradrenaline.

Noradrenaline spillover is considered the standard measurement for global sympathetic nerve firing rate (*9*) and can be measured using a radiotracer method. This method involves the continuous intravenous infusion of a tracer dose of radioactive noradrenaline. The spillover rate represents the amount of noradrenaline that enters the plasma. For the infusion rate of radioactive noradrenaline, the following relationship holds at a steady state: noradrenaline spillover rate = infused radioactive noradrenaline/plasma noradrenaline specific radioactivity.

This technique can be used not only to assess total-body spillover of noradrenaline but also to measure spillover in the heart by intracoronary infusion of radioactive noradrenaline and by sampling of the coronary sinus. The spillover from the heart can be calculated by means of the Fick principle: cardiac noradrenaline spillover = (coronary sinus − radioactive noradrenaline) + (radioactive noradrenaline × cardiac noradrenaline fractional extraction) × coronary sinus plasma flow. This method, however, cannot discriminate between increased neuronal release and reduced neuronal uptake. Furthermore, because cardiac catheterization is needed, the invasive nature of this method is a major drawback.

Sympathetic Nervous System at a Postsynaptic Level

Indirect information concerning the postsynaptic sympathetic activity can be obtained in vitro by determining β-adrenoceptor density in an endomyocardial biopsy. One hypothesis is that the sensitivity of the cardiac β-adrenoceptors can be measured in vivo by assessing the chronotropic and inotropic responses to endogenous and exogenous β-adrenoceptor agonists. For example, a blunted chronotropic response to isoproterenol is often seen in patients with heart failure and is related to unfavorable prognosis in these patients (*7*). However, these methods do not provide direct information on the density and activity of postsynaptic receptors and have limited clinical applications.

Sympathetic Nervous System at the Effector Level

The autonomic nervous system modulates heart rate variability. This physiologic effect can be assessed by means of ambulatory recorded electrocardiograms. For example, reduced heart rate variability has been observed in patients with chronic congestive heart failure (*8*). Power spectrum analysis may be performed to determine the contribution of sympathetic nerve activity to fluctuations in sinus rhythm. This power spectrum represents the distribution of the total variance in the signal over the different constituent frequencies. Low-frequency oscillations (0.04–0.15 Hz) are partially evoked by the sympathetic nervous system, suggesting that they may provide information on sympathetic nervous activity at a postsynaptic level. In chronic heart failure, tachycardia is usually accompanied by a reduction in total power in the heart rate variability spectrum. The low-frequency power expressed as a percentage of total power is a good indicator of sympathetic modulation of heart rate and has been shown to be increased in patients with chronic heart failure.

However, arrhythmias strongly influence the power spectrum, and only patients with sinus rhythm can be studied with this technique. Furthermore, quantitative assessment of sympathetic activity by this technique is difficult because heart rate variability is an end-organ response, which is determined not only by nerve firing and electrochemical coupling but also by cardiac β-adrenoceptor sensitivity and postsynaptic signal transduction. These phenomena may explain the frequently observed absence of correlation between heart rate variability and cardiac noradrenaline spillover.

RADIOPHARMACEUTICALS FOR CARDIAC NEUROTRANSMISSION ASSESSMENT

Radiotracers for scintigraphic imaging of cardiac neurotransmission have been developed by radiolabeling of the

neurotransmitters or their structural analogs or false neurotransmitters. Binding characteristics, selectivity, and binding reversibility determine the suitability of a given agent. Furthermore, radiochemical purity, and specific activity required to minimize occupation of binding sites by nonlabeled molecules, as well as pharmacologic effects in patients, have to be defined in the process of validation of neurotransmission radiopharmaceuticals for in vivo imaging.

Of the many radiopharmaceuticals that have been designed and tested to assess cardiac neurotransmission, the most commonly used are the following (Table 1; Fig. 2): at a presynaptic level, ^{18}F-fluorodopamine is available to assess norepinephrine synthesis, and ^{11}C-hydroxyephedrine, ^{11}C-ephedrine, and ^{123}I-metaiodobenzylguanidine (MIBG) are available to assess presynaptic reuptake and storage by PET and SPECT; at a postsynaptic level, β-blockers such as ^{11}C-CGP and ^{11}C-carazolol are available to assess β-adrenoceptor expression and density. The quantification of neurotransmitter synthesis and transport by PET requires tracer kinetic modeling. Typically, presynaptic norepinephrine reuptake function is assessed by calculation of the distribution volume of tracers using compartment models and nonlinear regression analysis to calculate influx and efflux rate constants. Myocardial adrenoceptor density (B_{max}) may be measured by injection of different amounts of radioactivity and cold substance, assessment of input function and estimation of metabolites, and graphic analysis.

^{18}F-Fluorodopamine

^{18}F-fluorodopamine is taken up in sympathetic nerve terminals and transported into axoplasmic vesicles, where it is converted into ^{18}F-fluoronorepinephrine and stored (*10*). During sympathetic stimulation, ^{18}F-fluoronorepinephrine is released from sympathetic nerve terminals similarly to ^{3}H-norepinephrine. 6-^{18}F-fluorodopamine can be synthesized from 6-^{18}F-fluorodopa by enzymatic decarboxylation using an L-amino acid decarboxylase (*11*). A direct synthesis method using a modification of the high-yield radiofluorodemercuration used in the synthesis of 6-^{18}F-fluorodopa can also be applied. The specific activities of the 6-^{18}F-fluorodopamine obtained by these synthesis methods typically range from 7,400 to 29,600 MBq/mmol (*10*,*11*).

Cardiac ^{18}F-fluorodopamine images can be analyzed by drawing regions of interest within the ventricular wall using a composite of the images for each plane. In computing time–activity curves, the logs of the concentrations of radioactivity, adjusted for the dose per kilogram of body weight, in the left ventricular myocardium and in arterial blood can be expressed as a function of time after injection of the radiotracer. The specific activity of ^{18}F-fluorodopamine at the time of injection and the assayed plasma concentrations of ^{18}F-fluorodopamine can be used to estimate the proportions of the total plasma radioactivity that are due to ^{18}F-fluorodopamine and its metabolites. Exponential curve fitting may be used to describe the relationships between time and radioactivity concentrations in myocardium, blood, and plasma. Differences between estimated and empiric values can be assessed graphically. The reported mean concentration of ^{18}F-fluorodopamine in the left ventricular myocardium peaks at 5–8 min after infusion, being 10.2 ± 67 nCi × kg/mL × mCi in healthy volunteers (*11*).

^{11}C-Hydroxyephedrine and ^{11}C-Epinephrine

^{11}C-hydroxyephedrine is a false neurotransmitter that has the same neuronal uptake mechanism as norepinephrine,

TABLE 1
Most Commonly Used Radiopharmaceuticals for Cardiac Neurotransmission Imaging

Targeted process	Radiopharmaceutical	Imaging and parameters	References
Presynaptic uptake-1 and storage	^{123}I-MIBG	Planar/SPECT Heart-to-mediastinum ratio Wash-out rate	*6,17–34,36,38,40,47–53,55–68,78–86*
Transport and storage into axoplasmic vesicles	^{18}F-fluorodopamine	PET Peak myocardial concentration	*10,11,35,72*
Presynaptic uptake-1 and storage	^{11}C-HED (hydroxyephedrine)	PET Retention fraction Volume distribution	*12,13,15,16,37,39,69,70,75,76*
Presynaptic uptake-1 and storage and metabolism	^{11}C-EPI (epinephrine)	PET Retention fraction Volume distribution	*14,15*
Postsynaptic adrenoceptor density	^{11}C-CGP (4-(3-*t*-butylamino-2-hydroxypropoxy)-benzimidazol-1)	PET Cardiac B_{max}	*24–26,42,43,69,70,75–77*
Postsynaptic adrenoceptor density	^{18}F-fluorocarazolol	PET Cardiac B_{max}	*27,28*
Postsynaptic muscarinic receptor density	^{11}C-MQNB (methylquinuclidinyl benzylate)	PET Cardiac B_{max}	*29,30*

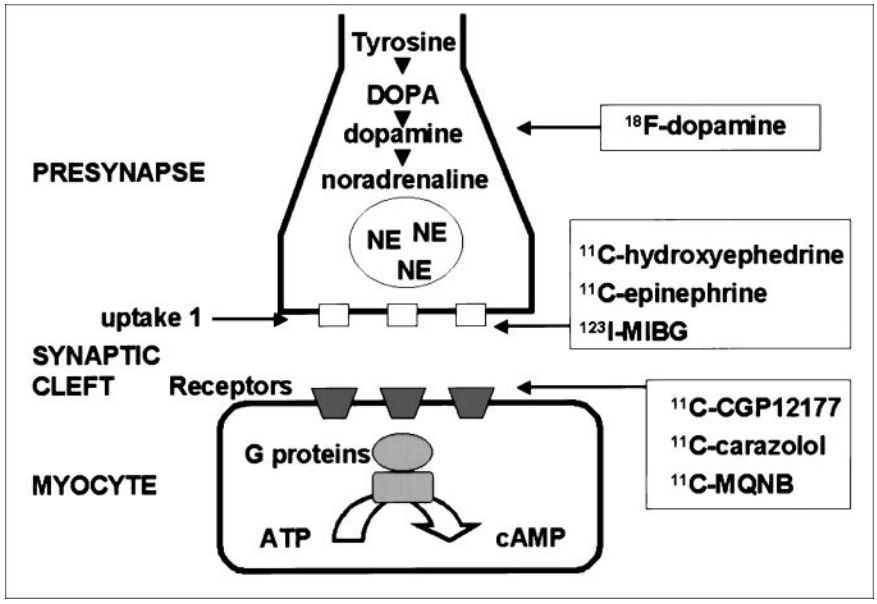

FIGURE 2. Most commonly used radioligands for assessment of cardiac pre- and postsynaptic processes. ATP = adenosine triphosphate; DOPA = dihydroxyphenylalanine; NE = norepinephrine.

through neuronal uptake-1, but is not degraded by monoamine oxidase and catechol methyltransferase, the enzymes responsible for the metabolism of norepinephrine in the heart (*12*). The storage and release properties, however, seem to differ from those of the physiologic neurotransmitters (*13*). ^{11}C-epinephrine may be a more physiologic tracer for the evaluation of presynaptic sympathetic nerve function regarding uptake mechanism, vesicular storage, and metabolism (*14*). ^{11}C-epinephrine is rapidly transported into the presynaptic nerve terminal through uptake-1 and is stored in the vesicles similarly to norepinephrine. ^{11}C-hydroxyephedrine and ^{11}C-epinephrine can be synthesized with chemical purity $>$ 95% and specific activity from 33,300 to 74,000 GBq/mmol (*15*). After correction for the contribution of ^{11}C-labeled metabolites, the calculated fraction of intact tracers can be plotted as a function of time. The corrected blood time–activity curve is used as the arterial input function for the calculation of myocardial retention of tracers. The retention fraction (L/min) can be calculated for each region by dividing the tissue ^{11}C concentration at 60 min by the integral of the radiotracer concentration in arterial blood from the time of injection to the end of the last scan: retention = $Ct(T_1{:}T_2)/\int^{T2} C_b(t)dt$, where $Ct(T_1{:}T_2)$ is tissue activity in the image frame between T_1 and T_2 (MBq/mL tissue), and C_b is blood activity (MBq/mL blood) integrated from time = 0 to time = T_2. Cardiac images can be analyzed by volumetric sampling procedures to generate time–activity curves and polar maps to assess homogeneity of myocardial tracer distribution (*14–16*). Volume distribution for ^{11}C-hydroxyephedrine in healthy volunteers has been reported to be 71 ± 19 mL/g of tissue. Myocardial retention fractions of ^{11}C-hydroxyephedrine and ^{11}C-epinephrine in healthy volunteers at 5 min after injection have been reported to be 0.24 ± 0.02 and 0.29 ± 0.02, respectively (*15*).

MIBG

Guanethidine is a potent neuron-blocking agent that acts selectively on sympathetic nerve endings (*17*). By the modification of this compound into MIBG, the affinity for neuronal uptake sites is increased. MIBG was labeled with ^{123}I to enable scintigraphic visualization of the sympathetic nervous system in humans (*18*), providing the first radiopharmaceutical for the assessment of cardiac neurotransmission by SPECT. The first clinical application of ^{123}I-MIBG was imaging of the adrenal medulla and neoplasms originating from the neural crest, such as pheochromocytoma and neuroblastoma (*19*). ^{123}I-MIBG scintigraphy also showed a striking uptake in the heart, because of its dense sympathetic innervation. In 1980, the potential use of ^{123}I-MIBG in myocardial imaging was first suggested, although at that time no information was available on the physiology of cardiac ^{123}I-MIBG uptake and its metabolism under different conditions in humans (*18*). Much work has been done to elucidate the mechanism by which the sympathetic nerve endings take up ^{123}I-MIBG. MIBG and noradrenaline have been shown to have similar molecular structures and to use the same uptake and storage mechanisms in the sympathetic nerve endings (*6,20–22*).

Neuronal uptake of ^{123}I-MIBG is achieved mainly through the sodium- and energy-dependent uptake-1 mechanism, which is characterized by a temperature dependency, a high affinity (a K_m [μmol/L] of 1.22 ± 0.12 for MIBG and 1.41 ± 0.50 for noradrenaline), and a low capacity (a V_m [pmol/10^6 cells/10 min] of 64.3 ± 3.3 for MIBG and 36.6 ± 7.2 for noradrenaline). Sisson et al. (*20,21*) showed in animal experiments that the kinetics of ^{125}I-MIBG mimicked those of ^{3}H-noradrenaline under different conditions. In these experiments, yohimbine, an α_2-adrenoceptor antagonist, was used to increase sympathetic nerve function, whereas clonidine was used to induce the opposite effect.

Sodium-independent neuronal uptake of MIBG has also been reported. This nonneuronal uptake-2 mechanism dominates at higher concentrations of the substrate and is probably the result of passive diffusion. The relative role of each uptake mechanism depends on the plasma concentration of MIBG. However, neuronal uptake is predominantly determined by the uptake-1 mechanism because an extremely small quantity of MIBG is usually injected for diagnostic scintigraphy. Typically, 1 standard dose of 185 MBq contains 6.25×10^{-9} g MIBG. Recently, the use of no-carrier-added MIBG has been reported to improve image quality (*23*).

^{11}C-CGP

Lipophilic antagonists of β-adrenoceptors such as iodopindolol have been used in in vitro studies. Lipophilic molecules such as ^{11}C-propranolol cannot be used to study the heart in vivo because of high accumulation in the lungs. CGP-12177 (4-(3-*t*-butylamino-2-hydroxypropoxy)-benzimidazol-1) is a hydrophilic antagonist that binds to the receptor with high affinity (0.3 nmol/L) (*24*). Because of high hydrophilicity, CGP-12177 selectively identifies cell-surface β-adrenoceptors that are coupled to adenylate cyclase. CGP can be labeled with ^{11}C using CGP-17704 as a precursor and ^{11}C-phosgene. To quantitatively assess the concentration of receptor sites, one must use a mathematic model (*24–26*). The model parameters, including the receptor concentration and the kinetic rate constants, can be derived from experimental data using a kinetic or graphic method. The kinetic method is based on a fitting procedure and needs to measure the input function, which is hampered by the presence of metabolites. Furthermore, the kinetic method needs to maintain a balance between the respective complexities of the model structure and of the experimental protocol. On the other hand, the graphic methods are based on simplifying hypotheses. A graphic method based on the injection of a tracer dose of CGP, followed by injection of radioligand with a low specific activity and an excess of unlabeled CGP, which does not require measurement of the input function, has been proposed (*24*). With this approach, values of B_{max} have been reported to be 10 ± 3 pmol/g of tissue in healthy volunteers, with a dissociation constant of 0.014 ± 0.002 min^{-1}.

^{18}F-Fluorocarazolol

Carazolol is a lipophilic, nonselective β-adrenoceptor antagonist to the β-1 and β-2 receptors and can be labeled with ^{11}C and ^{18}F (*27*). Uptake in the target organs, such as the heart, is substantial and can be blocked and displaced by propranolol in a way that suggests that fluorocarazolol and propranolol compete for binding to the same receptor sites. The in vivo binding is stereoselective because the *R*-isomer does not accumulate in the target organs (*28*). ^{18}F-fluorocarazolol can be synthesized by reacting the precursor *S*-desisopropylcarazolol with ^{18}F-fluoroacetone and high-performance liquid chromatography purification. The specific activity may average 55,500 GBq/mmole, with a radiochemical purity > 99%. After correction for metabolites in plasma, time–activity curves from the heart and lungs can be normalized to injected dose and body weight. Myocardial tissue-to-plasma concentration ratios of fluorocarazolol in healthy individuals reach a plateau of 18 ± 1 in the heart at 45 min after injection of the radiotracer. During the slow kinetic phase, maximal concentrations in the heart range from 0.03 to 0.085 pmol/mL (*28*).

^{11}C-Methylquinuclidinyl Benzilate

Methylquinuclidinyl benzilate (MQNB) is a highly specific hydrophilic antagonist of muscarinic receptors and can be labeled with ^{11}C. The stimulation of local muscarinic receptors inhibits norepinephrine release from adrenergic nerve terminals. Although present on sympathetic nerve endings in a prejunctional distribution, muscarinic receptors play a role in neurotransmission within the intrinsic cardiac sympathetic nervous system. MQNB can be labeled with ^{11}C by methylation of quinuclidinyl benzylate with ^{11}C-methyl iodide, with a specific radioactivity ranging from 12 to 80 GBq/μmol (*29,30*). Left ventricular muscarinic receptors can be quantified after PET imaging with a mathematic model based on a multiinjection protocol of labeled and unlabeled ligand. The input function can be derived from a region of interest drawn within the left ventricular cavity. Time–activity curves can be generated for different left ventricular regions after correction for decay and expressed as pmol/mL after dividing by specific radioactivity at time 0. After compartmental modeling, the B_{max} values reported in healthy volunteers were 25 ± 7.7 pmol/L, with a dissociation constant of 2.2 ± 1 pmol/mL without significant differences in the septal, anterior, and lateral regions of the left ventricle (*30*).

IMAGING TECHNIQUES

Planar and Tomographic Imaging of the Heart with MIBG

Planar imaging has commonly been used to determine cardiac MIBG uptake. Myocardial uptake and distribution are visually assessed. A semiquantitative measurement of myocardial MIBG uptake can be obtained by calculation of a heart-to-mediastinum ratio (*6*). However, this technique has some limitations: the superposition of noncardiac structures such as the lung and mediastinum may preclude optimal visualization, and superposition of myocardial segments and motion artifacts interferes with regional assessment of radioligand uptake. SPECT imaging may overcome these disadvantages, although in some pathophysiologic conditions, myocardial MIBG uptake may be severely reduced, hampering the obtention of tomographic slices of the heart.

The standard procedure is as follows. Thirty minutes after thyroid blockade by oral administration of 500 mg potassium perchlorate, approximately 370 MBq ^{123}I-MIBG are administered intravenously. Planar scintigraphic images and SPECT studies of the heart are acquired 20 min (early

image) and 4 h (delayed image) after injection. A 20% window is usually used, centered over the 159-keV ^{123}I photopeak. Planar images are acquired in anterior and 45° left anterior oblique views of the thorax and stored in a 128 × 128 matrix. MIBG uptake is semiquantified by calculating a heart-to-mediastinum ratio after drawing regions of interest over the mediastinum in the anterior view and over the myocardium in the left anterior oblique view. Average counts per pixel in the myocardium are divided by average counts per pixel in the mediastinum. The intraobserver variability of the heart-to-mediastinum ratio is <2%, and the interobserver variability is <5%. A heart-to-mediastinum ratio > 1.8 is considered normal. The washout rate from initial to delayed images is <10% in healthy individuals (*31*,*32*). SPECT studies can be obtained by a single pass of 60 steps at 30 s per step (64 × 64 matrix), starting at the 45° right anterior oblique projection and proceeding counterclockwise to the 45° left posterior oblique projection. The data are reconstructed in short-axis, horizontal long-axis, and vertical long-axis views, and scatter or attenuation correction may be applied. For visual evaluation of SPECT slices, reductions in the MIBG concentration in given myocardial segments can be scored using a point scale. In addition, polar maps can be constructed from short-axis images and can be compared with those of healthy individuals (Figs. 3 and 4).

Quantitative assessment of the cardiac uptake of MIBG in the heart, by comparing the cardiac count density with the count density of a reference region such as the mediastinum, is hampered by several variables. First, tissue attenuation is nonuniform for intrathoracic organs because tissue density and, therefore, the attenuation coefficient vary. This nonuniform attenuation can be corrected theoretically using an iterative reconstruction algorithm or by constructing individual attenuation maps during acquisition using a line source. Second, photons that scatter within the patient are

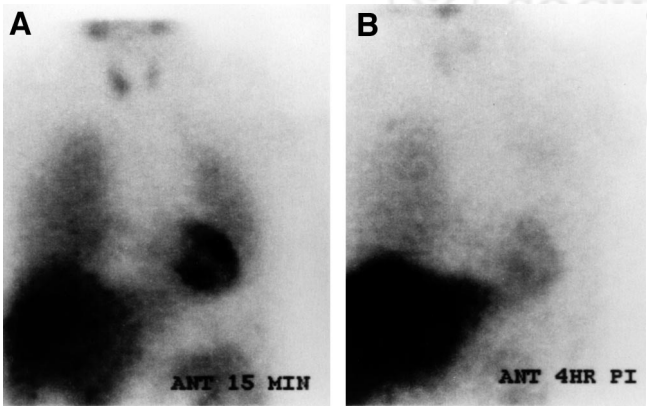

FIGURE 3. Planar cardiac ^{123}I-MIBG images of cancer patient after chemotherapy. Intensity of cardiac MIBG uptake can be assessed by comparing activity in heart with activity in mediastinum. Accelerated washout of MIBG is seen between early (A) and delayed (B) images after chemotherapy. ANT = anterior view; PI = postinjection.

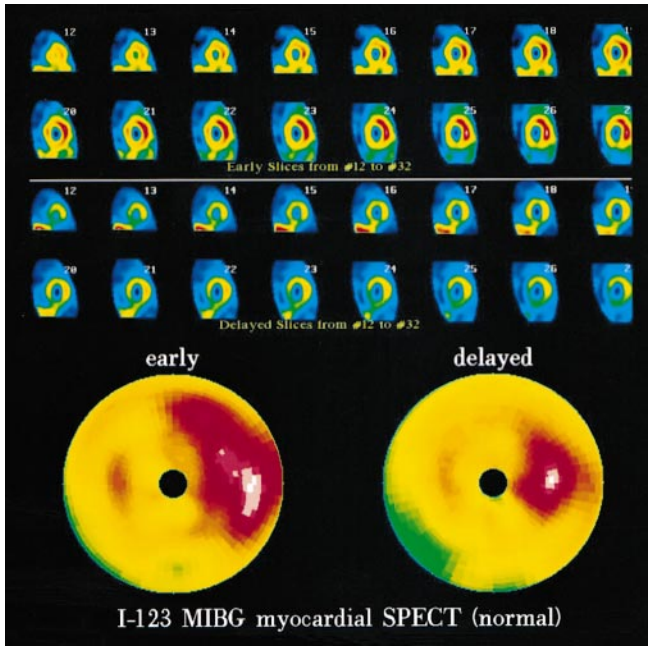

FIGURE 4. SPECT MIBG study of healthy volunteer. Short-axis tomograms and reconstructed polar maps show normal MIBG distribution and washout.

often indistinguishable from unscattered photons with respect to their photon energy. These scattered photons contribute to a further loss of spatial resolution. For ^{123}I-MIBG SPECT, a limiting factor is the number of counts acquired. Therefore, dose and acquisition time should be maximized. Procedures to limit the effects of these factors will improve image quality, that is, image resolution and contrast.

Somsen et al. (*33*) and Somsen (*34*) have developed a method in which the count density in the left ventricular cavity is used as a reference. Volumes of the myocardium and the left ventricular cavity are reconstructed from SPECT acquisitions. The count density in the left ventricular cavity is calibrated by the ^{123}I activity in a venous blood sample drawn at the time of the acquisition. Subsequently, cardiac ^{123}I-MIBG uptake can be calculated according to the following equation: cardiac ^{123}I-MIBG uptake = (myocardial count density/cavity count density) × venous blood sample (Bq/mL).

PET Imaging

PET imaging protocols vary according to the radiotracer characteristics and the available instrumentation. Obtained volumetric datasets are realigned according to standardized axes. Physiologic parameters can be assessed by applying tracer kinetic models to quantitative datasets (Fig. 5). Region-of-interest analysis of the activity concentration inside the left ventricular cavity yields the time–activity curve of arterial blood and allows assessment of the arterial input function. Continuous thoracic PET scanning is performed for up to 3 h after ^{18}F-fluorodopamine infusion. The total scanning time is divided into intervals of 5–30 min, and the tomographic results of each interval are assessed. Scan

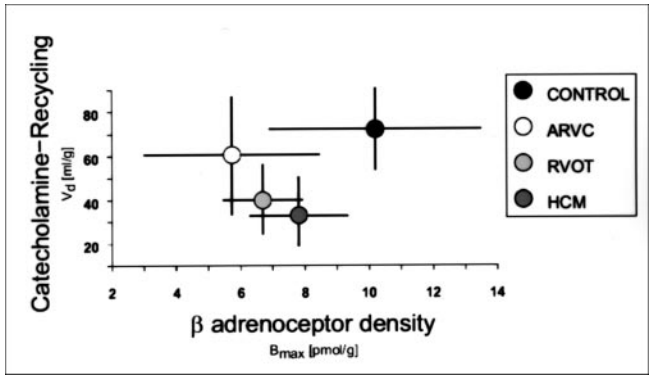

FIGURE 5. PET characterization of presynaptic volume distribution of neurotransmitter (V_d of ^{11}C-hydroxyephedrine) and postsynaptic receptor density (B_{max} measured by ^{11}C-CGP) in healthy volunteers (CONTROL) and patients with arrhythmogenic right ventricular cardiomyopathy (ARVC), right ventricular outflow tract (RVOT), and hypertrophic cardiomyopathy (HCM). Circles represent mean values; crosses represent SDs.

sequences may consist of 5 frames × 1 min, 5 frames × 5 min, 4 frames × 15 min, and 3 frames × 30 min. PET scanning of ^{11}C-hydroxyephedrine and ^{11}C-epinephrine usually lasts for 60 min. Scan sequences may consist of 15 frames: 6 × 30 s, 2 × 60 s, 2 × 150 s, 2 × 300 s, 2 × 600 s, and 1 × 1,200 s. With ^{11}C-CGP, continuous thoracic scanning, recording data in list mode, is typically performed for 1 h after infusion. With ^{18}F-fluorocarazolol, acquisition protocols after infusion may consist of 8 frames × 15 s, 4 frames × 30 s, 4 frames × 1 min, 4 frames × 2 min, 6 frames × 4 min, and 2 frames × 10 min. For ^{11}C-MQNB, data recording starts with the first injection. Sixty sequential images may be acquired, using 1 of the cross-sections and reconstruction according to the specific protocol applied. Scan sequences may consist of 22 frames—8 × 15 s, 4 × 30 s, 2 × 60 s, and 8 × 150 s—after each infusion.

CLINICAL APPLICATIONS

Primary Cardioneuropathies

Dysautonomias. Derangements of sympathetic and parasympathetic nervous system function are frequently encountered in neurology and cardiology. Autonomic hypofunction can be caused by several drugs and disease-associated polyneuropathies such as diabetes and amyloidosis. Autonomic failure may also occur without an identifiable cause or sometimes in relation to a disease in which dysautonomia is unlikely. A consensus statement by the American Autonomic Society and the American Academy of Neurology distinguishes 3 forms of primary disautonomia: pure autonomic failure, defined as a sporadic, idiopathic cause of persistent orthostatic hypotension and other manifestations of autonomic failure that occur without other neurologic features; Parkinson's disease with autonomic failure; and multiple-system atrophy. However, distinguishing between Parkinson's disease with autonomic failure and some forms of multiple-system atrophy is difficult, and physiologic and neurochemical tests often fail to properly separate the different forms of dysautonomia.

Goldstein et al. (*10*,*35*) have used PET scanning with ^{18}F-fluorodopamine to examine cardiac sympathetic innervation in patients with different types of dysautonomia. In light of the PET findings, they proposed a new pathophysiologic classification of dysautonomias in which sympathetic neurocirculatory failure results from peripheral sympathetic denervation or decreased or absent sympathetic signal traffic. The results of PET scanning are related to central degeneration, to responsiveness to treatment with levodopa–carbidopa, and to signs of sympathetic neurocirculatory failure, with orthostatic hypotension and abnormal blood pressure responses associated with Valsalva's maneuver. Patients with pure autonomic failure or parkinsonism and sympathetic neurocirculatory failure have no myocardial ^{18}F-fluorodopamine uptake or cardiac norepinephrine spillover, indicating loss of myocardial sympathetic-nerve terminals. Patients with the Shy-Drager syndrome have increased levels of ^{18}F-fluorodopamine activity, indicating intact nerve terminals and absent nerve traffic. Patients with dysautonomia without sympathetic neurocirculatory failure have normal levels of ^{18}F-fluorodopamine activity in the myocardium and normal rates of cardiac norepinephrine spillover. ^{18}F-fluorodopamine PET studies in combination with neurochemical tests and clinical observations support this new clinical pathophysiologic classification of dysautonomias, with enhanced diagnostic differentiation between multiple-system atrophy, Shy-Drager syndrome, parkinsonism with autonomic failure, and peripheral autonomic failure (*35*).

Heart Transplantation. During orthotopic heart transplantation, the entire recipient heart is excised except for the posterior atrial walls, to which the donor atria are anastomosed. During the process, the allograft becomes completely denervated. Lack of autonomic nerve supply is associated with major physiologic limitations. The inability to perceive pain does not allow symptomatic recognition of accelerated allograft vasculopathy, and heart transplant patients often experience acute ischemic events or left ventricular dysfunction or die suddenly. In addition, denervation of the sinus node does not allow adequate acceleration of heart rate during stress and efficient increase in cardiac output. Furthermore, loss of vasomotor tone may adversely affect the physiologic alterations in blood flow, produce altered hemodynamic performance at rest and during exercise, and decrease exercise capacity. Scintigraphic uptake of ^{123}I-MIBG and ^{11}C-hydroxyephedrine supports the concept that spontaneous reinnervation takes place after transplantation (*36*–*39*). All studies performed up to 5 y after heart transplantation suggest that reinnervation is likely to be a slow process and occurs only after 1 y after transplantation (*40*).

Sympathetic reinnervation, measured by regional distribution and intensity of myocardial MIBG uptake, increases with time after transplantation, with a positive correlation

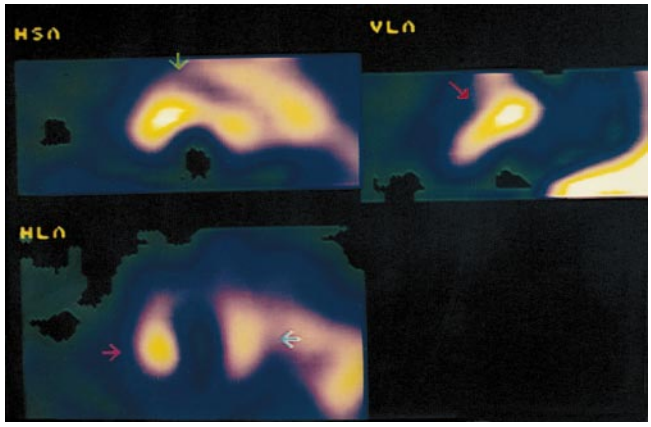

FIGURE 6. SPECT images of MIBG distribution in patient presenting with partial reinnervation after heart transplantation. MIBG activity (arrows) is seen in anterobasal segments of myocardium. HLA = horizontal long axis; HSA = horizontal short axis; VLA = vertical long axis.

between heart-to-mediastinum rates and time after transplantation. Serial MIBG studies over time show that reinnervation begins from the base of the heart and spreads toward the apex (Fig. 6). MIBG uptake is seen primarily in the anterior, anterolateral, and septal regions. MIBG uptake is usually not apparent in the posterior or inferior myocardial regions, except for some basal posterior localization. Complete reinnervation of the transplanted heart is not seen on scintigraphic studies, even up to 12 y after transplantation. Early vasculopathy may inhibit the process of sympathetic reinnervation of the transplanted heart. The relationship between reinnervation status and graft vasculopathy deserves further investigation and may help to characterize subsets of transplant patients with different clinical outcomes.

In a recent PET perfusion and sympathetic reinnervation study of heart transplant patients, Di Carli et al. (*39*) showed that blood flow increases in response to sympathetic stimulation in the territory of the left anterior descending artery. This territory has the highest uptake of ^{11}C-hydroxyephedrine, whereas in other territories, increase in flow and uptake of ^{11}C-hydroxyephedrine is minor. This study also showed that basal flow in transplant recipients is similar in all coronary territories despite differences in sympathetic reinnervation, suggesting that cardiac-efferent adrenergic signals play an important role in modulating myocardial blood flow during activation of the sympathetic nervous system.

Idiopathic Ventricular Tachycardia and Fibrillation. In patients presenting with idiopathic ventricular tachycardia and fibrillation, no structural or functional abnormalities of the myocardium can be shown by conventional imaging and clinical testing. Early diagnosis and treatment are of clinical importance because ventricular fibrillation is the most common arrhythmia at the time of sudden death (*41*). Typical arrhythmias in these patients can be provoked by physical or mental stress or by catecholamine application. Schafers et al. (*42*), using ^{123}I-MIBG, ^{11}C-hydroxyephedrine, and ^{11}C-CGP, showed that in patients with idiopathic right ventricular outflow tract tachycardia, both the presynaptic myocardial catecholamine reuptake and the postsynaptic myocardial β-adrenoceptor density were reduced despite normal blood catecholamine levels (Fig. 7). The maximal binding capacity of the β-adrenoceptor antagonist was reduced in patients with right ventricular outflow tract tachycardia, in comparison with healthy volunteers (6.8 ± 1.2 vs. 10.2 ± 2.9 pmol/g) (*43*). These scintigraphic findings represent the only demonstrable myocardial abnormality in patients with idiopathic tachycardia and fibrillation and suggest that myocardial β-adrenoceptor downregulation in these patients occurs subsequent to increased local synaptic catecholamine levels caused by impaired catecholamine reuptake (*43*).

Secondary Cardioneuropathies

Dilated Cardiomyopathies. After the onset of myocardial failure, enhanced sympathetic nervous system activity plays an important role in supporting the cardiovascular system by increasing heart rate, contractility, and venous return. Blood pressure to preserve organ perfusion is supported by systemic arterial constriction, but on the other hand, increased sympathetic activity has deleterious effects on the cardiovascular system (*7*,*9*). Vascular constriction and increased salt and water retention by the kidneys increase the energy requirement of the myocardial wall. Altered sympathetic cardiac adrenergic function may also cause arrhythmias, desensitization of postsynaptic β-adrenoceptors, and activation of other neurohumoral systems, such as the renin–angiotensin system, which may themselves exert adverse effects and contribute to progression of myocardial dysfunction. In addition, prolonged exposure to norepinephrine may contribute to disease progression by acting directly on the myocardium to modify cellular phenotype and result in myocyte death (*44*,*45*).

In patients with dilated cardiomyopathies, because of the increased concentration of circulating catecholamines re-

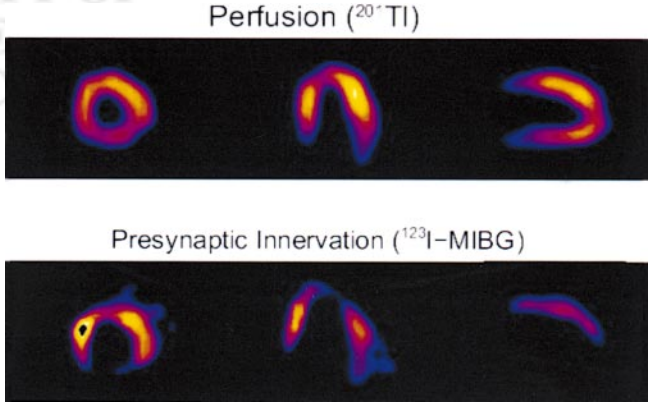

FIGURE 7. SPECT images of resting perfusion (^{201}Tl) and sympathetic presynaptic innervation (^{123}I-MIBG) of left ventricular myocardium in patient with idiopathic ventricular tachycardia. Typically, regional innervation in segments of inferior wall is blunted, whereas same segments show no perfusion abnormality.

sulting from heart failure, the myocardial responsiveness to β-adrenoceptor agonists is blunted. Frequently, alterations of cardiac sympathetic innervation contribute to fatal outcomes in patients with heart failure. Merlet et al. (*46–48*), studying patients with functional classes II–IV and <40% left ventricular function, and using transplantation and cardiac or noncardiac death as endpoints, showed that the only independent predictors of mortality were low MIBG uptake and left ventricular ejection fraction. In addition, MIBG uptake and circulating norepinephrine concentration were the only predictors for life duration when using multivariate life table analysis. Therefore, impaired cardiac adrenergic innervation as assessed by MIBG imaging seems to be strongly related to mortality in patients with heart failure (Figs. 8 and 9). Along the same line, Maunoury et al. (*49*) found that cardiac adrenergic neuronal function was impaired in children with idiopathic dilated cardiomyopathy, although that particular study did not have sufficient follow-up for assessment of prognosis. Patients with congestive cardiomyopathy typically have accelerated washout rates (>25% from 15 to 85 min), in comparison with healthy volunteers (<10%). Momose et al. (*50*) assessed the prognostic value of washout rate in heart failure patients and found that it was the most powerful independent predictor of prognosis and that a threshold of 52% clearly separated negative outcome from survival. Cohen-Solal et al. (*51*) showed that MIBG parameters correlated with other predictors of prognosis such as peak volume of oxygen use. Cardiac MIBG SPECT has also been used to assess changes in cardiac sympathetic neuronal uptake function caused by pharmacologic intervention (*52*). Somsen et al. (*33*) showed that enalapril improved cardiac sympathetic uptake function but did not affect plasma noradrenaline levels in a group of patients with heart failure, supporting the concept that a restoration of cardiac neuronal uptake of noradrenaline is a benefit of enalapril treatment in these patients. Suwa et al. (*53*) prospectively evaluated whether MIBG myocardial imaging was useful in predicting responses to α-blocker therapy in patients with dilated cardiomyopathy. Heart-to-mediastinum ratios on early and delayed images were evaluated, as well as the percentage washout rate. The heart-to-mediastinum ratio on delayed images was a good predictor of the response to α-blocker therapy, with a threshold of 1.7 identifying responders to bisoprolol with a sensitivity of 91% and a specificity of 92%. These results indicate that the response to α-blocker therapy may be monitored with sequential quantitative MIBG studies (Fig. 10).

The concept that prolonged sympathetic hyperactivity is detrimental in chronic heart failure has been supported by

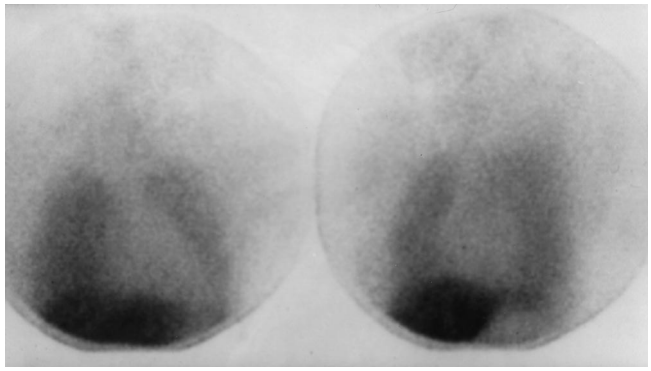

FIGURE 9. Planar MIBG images of patient with dilated cardiomyopathy and almost absent cardiac MIBG uptake. This pattern of denervation is associated with very poor outcome, and heart transplantation has to be considered.

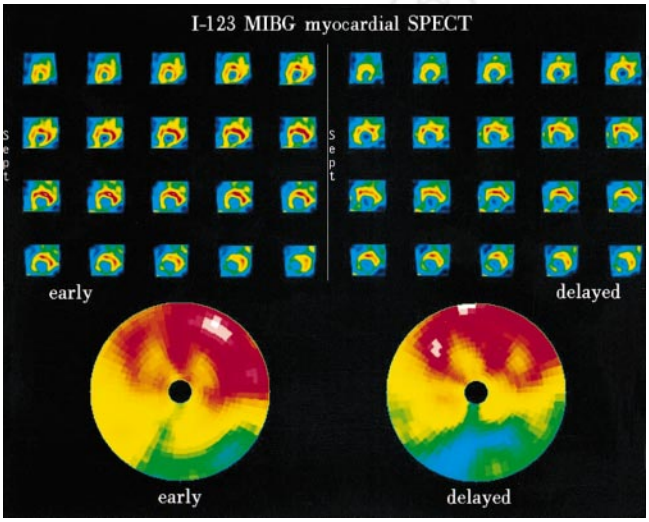

FIGURE 8. SPECT MIBG study of patient with dilated cardiomyopathy. Short-axis tomograms and reconstructed polar maps show decreased and heterogeneous myocardial MIBG activity.

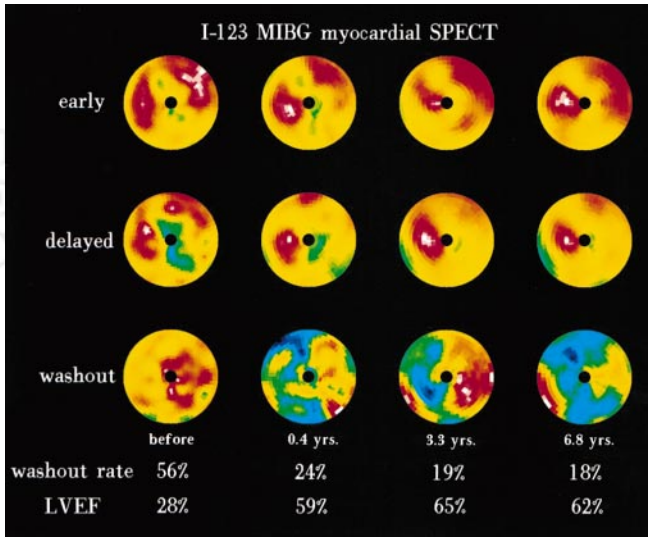

FIGURE 10. Sequential MIBG polar maps of patient who responded to α-blocker therapy. Studies were obtained before and at follow-up intervals after α-blocker administration. MIBG distribution improves over time, and washout rate is progressively less. Left ventricular ejection fraction (LVEF) improves from 28% to 65%.

trials that showed beneficial effects from angiotensin-converting enzyme inhibitors and β-adrenoceptor antagonists. Therefore, reduction of sympathetic nervous activity is considered an important target for drug treatment of heart failure. Several mechanisms may contribute to reduced β-adrenoceptor responsiveness in heart failure, such as downregulation of β-adrenoceptors, uncoupling of subtypes of β-adrenoceptors, upregulation of β-adrenoceptor kinase, increased activity of G protein, decreased activity of adenylyl cyclase, and increased nitric oxide. Myocardial remodeling involves hypertrophy and apoptosis of myocytes, regression to a fetal phenotype, and changes in the nature of the extracellular matrix. Noradrenaline seems to contribute to many of these changes by direct stimulation of adrenoceptors on cardiac myocytes and fibroblasts. The hypertrophic effect of noradrenaline is associated with the reexpression of fetal genes and the downregulation of several adult genes. Cardiac neurotransmission imaging can play a role in future trials to assess new forms of medical therapy for improving outcomes in heart failure.

The death of cardiac myocytes by apoptosis may contribute to pathologic remodeling. Apoptosis is a highly regulated sequence of molecular and biochemical events guided by a genetic program. Although apoptosis was thought not to occur in terminally differentiated cardiac myocytes, Narula et al. (*54*) showed that apoptosis was present in the myocardium of patients with end-stage dilated cardiomyopathy, leading to the concept that continuing loss of viable myocytes contributes to progressive myocardial failure. Several studies have suggested that the toxic effect of β-adrenoceptor stimulation is mediated in part by apoptosis. In cultured myocytes, exposure to noradrenaline for 24 h stimulates the frequency of apoptosis, which is inhibited by propranolol. In comparison, little is known about the effects of noradrenaline on the extracellular matrix, although noradrenaline stimulates the expression of transforming growth factors that regulate extracellular matrix proteins. Cardiac neurotransmission imaging can help to improve understanding of the mechanisms responsible for increased sympathetic activity in heart failure, and knowledge of how sympathetic overactivity exerts its deleterious actions will result in better therapy and outcome for patients with heart failure, which is still a major cause of disability and mortality and represents a major health problem despite therapeutic advances.

Coronary Artery Disease. Sympathetic nervous tissue may be more sensitive to the effects of ischemia than is myocardial tissue. Uptake of ^{123}I-MIBG has been shown to be significantly reduced in areas of myocardial infarction and of acute and chronic ischemia (*55–57*). A decrease in MIBG uptake in ischemic tissue represents loss of integrity in postganglionic, presynaptic neurons. Ischemia likely induces damage to sympathetic neurons, which may take a long time to regenerate, and repetitive episodes of ischemia likely result in a relatively permanent loss of MIBG uptake (Fig. 11). Early after infarction, sympathetic denervation in adjacent noninfarcted regions is frequently observed (*56*). Studies have shown that a transmural infarction produces acute sympathetic denervation in noninfarcted sites apical to the necrotic regions as measured by norepinephrine content and response to stellate stimulation. Nontransmural infarction may also lead to regional ischemic damage of sympathetic nerves but may spare subepicardial nerve trunks that course the region of infarction to provide a source of innervation to distal areas of the myocardium.

Minardo et al. (*58*) used ^{123}I-MIBG to show that the area of denervation extended beyond the region of infarction. McGhie et al. (*56*), evaluating patients with MIBG scintigraphy on day 10 after acute myocardial infarction, found that the area of reduced uptake was more extensive than the area of the thallium perfusion defect. These regions may be associated with spontaneous ventricular tachyarrhythmias after myocardial infarction (*59*). Sympathetic stimulation is known to lower the threshold of ventricular tachycardia and fibrillation during acute myocardial ischemia. Adrenergic denervation of viable myocardium results in denervation supersensitivity, with an exaggerated response of myocardium to sympathetic stimulation. Denervation supersensitivity is related to vulnerability to ventricular arrhythmias. Regional sympathetic denervation is possibly one of the mechanisms that renders patients with coronary artery disease susceptible to ventricular arrhythmias during myocardial ischemia. Reinnervation late after myocardial infarction in periinfarct regions has also been shown by reappearance

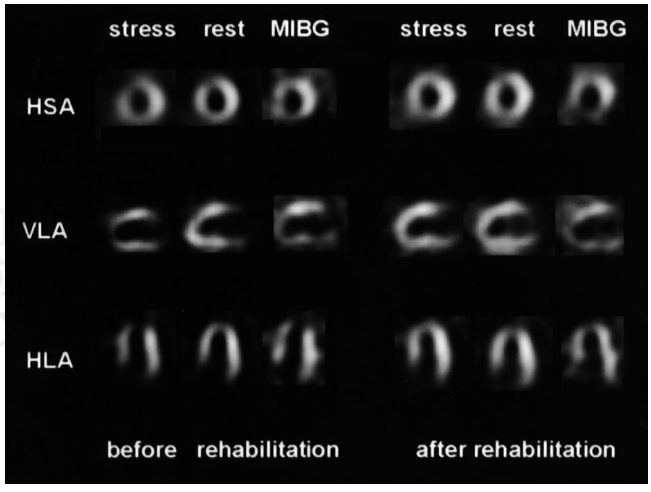

FIGURE 11. Myocardial exercise/rest perfusion studies (^{99m}Tc-tetrofosmin) and sympathetic innervation studies (^{123}I-MIBG) performed before and 6 mo after exercise rehabilitation in patient with coronary artery disease. Before rehabilitation, myocardial perfusion study shows anterior and apical ischemia. MIBG study shows decreased uptake in same territories. After rehabilitation, marked improvement in myocardial perfusion is seen, whereas sympathetic innervation study is similar to study before exercise rehabilitation, suggesting persistent neuronal damage after repetitive myocardial ischemia. HSA = horizontal short axis; VLA = vertical long axis; HLA = horizontal long axis.

of MIBG uptake by 14 wk after infarction (*60,61*). Reinnervation may be, in part, responsible for the return of function during this period. However, reinnervation may be incomplete as late as 3 mo after acute infarction. Hartikainen et al. (*60*) examined MIBG uptake at 3 and 13 mo after a first infarction and found no difference in MIBG activity over time within the infarcted zone but an increase in activity in the periinfarcted region without a change in perfusion.

The eventual concordance between the extent of MIBG defect at rest and perfusion defect at exercise in patients with coronary artery disease suggests that mild degrees of ischemia may be injurious to the integrity of myocardial sympathetic neurons (*62–65*). Correlation between the MIBG defect and the area at risk and the presence of angina further supports the concept of neuronal damage in the ischemic territory. Although association between MIBG defects and clinical angina can be explained as a consequence of ischemia, it is intriguing that the perception of pain occurs from the area that lacks sympathetic innervation. Because MIBG defects in the ischemic territory are not absolute, partial neuronal innervation may allow perception of chest pain. The MIBG studies in cardiac allograft recipients also support the finding of both susceptibility of sympathetic neurons to ischemia and adequacy of partial innervation for nociception. Reinnervation in transplant recipients is almost never complete; still, these patients can perceive pain. On the other hand, in all patients who sustain early episodes of allograft vasculopathy, reinnervation does not develop even up to 12 y after heart transplantation. This finding also supports the concept of extreme sensitivity of sympathetic innervation to ischemic stress—even greater than the sensitivity of the myocyte (*65–68*).

Hypertrophic Cardiomyopathy. Hypertrophic cardiomyopathy is genetically determined; however, autonomic dysfunction seems to play a role in the phenotypic expression. Several clinical features of hypertrophic cardiomyopathy suggest increased sympathetic outflow. The incidence of chest pain and myocardial hypercontractility, the propensity to ventricular arrhythmias and sudden death, and the beneficial effect of α-blockers suggest increased delivery of norepinephrine to myocardial adrenoceptors. Cardiac presynaptic catecholamine reuptake is impaired in hypertrophic cardiomyopathy, in association with reduced postsynaptic β-adrenoceptor density, suggesting an increased neurotransmitter concentration in the synaptic cleft. This increase can be shown by quantitative PET studies using ^{11}C-hydroxyephedrine and ^{11}C-CGP (*69,70*). An increased washout rate (>25%) between initial and delayed images has also been described in hypertrophic cardiomyopathy, secondary to activation of the sympathetic nervous system. The autonomic dysfunction in these patients is probably related to disease progression and, ultimately, heart failure (*71,72*). In patients studied with ^{13}N-ammonia and ^{18}F-fluorodopamine, the ^{18}F:^{13}N ratio is lower in hypertrophied than in nonhypertrophied regions (*72*), indicating decreased neuronal uptake of catecholamines in hypertrophied myocardium of patients with hypertrophic cardiomyopathy.

Arrhythmogenic Right Ventricular Cardiomyopathy. Fibrolipomatous degeneration of the right ventricular myocardium is the main structural abnormality in arrhythmogenic right ventricular cardiomyopathy. In these patients, the evidence of ventricular tachyarrhythmias and cardiac arrest that can be provoked during exercise or stress, and the sensitivity to catecholamines, strongly suggest that the sympathetic nervous system is involved in arrhythmogenesis (*73,74*). Studies with MIBG-SPECT and ^{11}C-hydroxyephedrine PET have shown that although the left ventricle is not involved in the disease, there is evidence of global and regional denervation in presynaptic catecholamine reuptake and storage of the left ventricle, as well as a reduction in the postsynaptic β-adrenoceptor density assessed by ^{11}C-CGP PET (*75,76*). B_{max} values for CGP of 5.9 ± 1.3 pmol/g of tissue have been shown in patients with arrhythmogenic cardiomyopathy versus 10.2 ± 2.9 pmol/g tissue in healthy volunteers (*77*). These findings suggest reduced activity of the noradrenaline transporter (uptake-1) with subsequent β-adrenoceptor downregulation and have a potential impact on diagnostic evaluation and therapeutic management of patients with arrhythmogenic right ventricular cardiomyopathy.

Diabetes Mellitus. The sympathetic nervous system appears to be activated during the early stages of diabetes, with elevated plasma catecholamine levels. This prolonged exposure to catecholamines leads to downregulation of adrenergic receptors and to alterations in adrenergic nerve fibers in the myocardium. Hyperglycemia and insulin deficiency may also contribute to the abnormalities in cardiac innervation in diabetes. Kim et al. (*78*) showed decreased ^{123}I-MIBG uptake associated with autonomic dysfunction in diabetic patients and a correlation between decreased cardiac MIBG uptake and increased mortality. MIBG scintigraphy seems more sensitive than autonomic nervous function tests for the detection of autonomic neuropathy in diabetes, particularly in early stages of the disease. Scognamiglio et al. (*79*) showed that impairment of cardiac sympathetic innervation, as revealed by MIBG studies, correlates with an abnormal response to exercise in diabetic patients and may contribute to left ventricular dysfunction before the appearance of irreversible damage and overt heart failure. Hattori et al. (*80*) reported that diabetic patients with scintigraphic evidence of severe myocardial denervation present with hyperreaction to dobutamine stress. This finding may, in part, explain the high incidence of sudden death in patients with advanced diabetes mellitus.

Hypertension. Scintigraphy of cardiac sympathetic innervation may play a role in the assessment of arterial and pulmonary hypertension. Morimoto et al. (*81*) investigated the relationship between hypertensive cardiac hypertrophy and cardiac nervous function before and after hypertensive therapy in patients with untreated essential arterial hypertension. A regional and global improvement in cardiac

sympathetic nervous function, as seen on ^{123}I-MIBG studies, appeared to be related to regression of hypertensive cardiac hypertrophy. Furthermore, in patients with pulmonary hypertension, the uptake ratio of MIBG between the interventricular septum and the left ventricular myocardium correlated with right ventricular overload (*82,83*). Therefore, scintigraphic assessment of the adrenergic nervous system may, conceivably, play a role in the multidisciplinary assessment and management of hypertension.

Drug-Induced Cardiotoxicity. MIBG studies have also been used to assess impairment of adrenergic innervation from anthracycline cardiotoxicity. Decreased myocardial MIBG uptake has been observed after administration of doxorubicin hydrochloride, with limited morphologic damage (*84*). In these studies, decreased myocardial MIBG uptake preceded deterioration of ejection fraction. MIBG uptake revealed a dose-dependent decline that could be caused by excessive compensatory hyperadrenergic washout from the myocardium or by direct adrenergic neuron damage. Hyperadrenergism seems unlikely because myocardial norepinephrine does not decline as plasma norepinephrine levels rise with increasing dose, suggesting a specific adrenergic neuron toxicity rather than a nonspecific response to an impairment in ventricular function. Valdés Olmos et al. (*85*) reported decreased myocardial MIBG uptake in patients with severely decreased ejection fraction after doxorubicin administration. A correlation with parameters derived from radionuclide angiocardiography suggested a global process of myocardial adrenergic derangement.

A decrease in myocardial MIBG uptake has also been reported regardless of the patient's functional status, suggesting a specific effect. Progressive myocyte necrosis during doxorubicin cardiotoxicity can be associated with cardiac neuroadrenergic tissue necrosis. In fact, the clinical course of doxorubicin cardiotoxicity suggests altered neuroendocrine physiology. This suggestion is supported by the observation of decreased adrenergic responsiveness and myocardial catecholamine stores with increased plasma catecholamines. The decrease in myocardial MIBG accumulation parallels the evolution of ejection fraction (*86*). When receiving intermediate cumulative doses of 240–300 mg/m^2, 25% of patients present with some decrease in MIBG uptake. At maximal cumulative doses, MIBG uptake decreases significantly, consistent with impaired cardiac adrenergic activity. A moderate to marked decrease in myocardial MIBG uptake at high cumulative doses was observed in all but 1 patient with a 10% decrease in ejection fraction (*86*). These data suggest that the assessment of drug-induced sympathetic damage can be used to select patients at risk of severe functional impairment and who may benefit from cardioprotective agents or changes in the schedule or administration technique of antineoplastic drugs.

FUTURE DIRECTIONS

The neuronal function of the heart is altered in many cardiac disorders, such as congestive heart failure, ischemia, cardiac arrhythmias, and certain cardiomyopathies. Cardiac neurotransmission imaging opens many possibilities for improving our understanding of the pathophysiology of the diseases, improving our selection of patients for various treatments, and improving our assessment of the results of therapy. As new drugs are shown effective for heart failure, the identification of markers predictive of drug efficacy for individual patients becomes increasingly important. Clearly, neuronal receptor function can be modulated with appropriate treatments; therefore, cardiac neurotransmission studies have great potential for affecting clinical decision making if the effectiveness of treatments can be assessed and predicted using SPECT or PET (*87,88*).

Future directions include developing new and more physiologic tracers, such as the non–carrier-added ^{123}I-fluoroiodobenzylguanidine (*89*), which is a more physiologic catecholamine analog than MIBG; implementing cardiac neurotransmission imaging in clinical practice; and focusing on the assessment and prediction of therapy. Also, development of ^{99m}Tc analogs of MIBG may lead to widespread application of cardiac neurotransmission imaging. In addition to PET tracers, SPECT ligands have to be developed for imaging the expression of adrenergic and muscarinic receptors. Labeling iododexetimide with ^{123}I for SPECT imaging has been attempted (*90*). Studies are needed to validate these tracers in clinical practice. Other types of receptors that can be targeted, and for which preliminary attempts indicate the feasibility of such an approach, include benzodiazepine receptors (*91*), which have a role in the modulation of cardiac vagal tone; angiotensin receptors; and receptors of endothelin and adenosine. Targeting of second messenger molecules, generated after binding of transmitters to their receptors, may offer a new way of assessing cardiac neurotransmission processes. Some radiotracers for the second messenger system are already on the horizon (*92*). Recent research on β-adrenoceptors has detected genetic variants that may have major implications in the future development of heart failure and early associated mortality. Early assessment of cardiac sympathetic innervation and early treatment to prevent heart failure in genetically predisposed individuals may be an important future application of cardiac neurotransmission imaging (*93*).

Several clinical goals need to be met to establish the clinical usefulness of cardiac neurotransmission imaging. Congestive heart failure accounts for a great burden on the Medicare budget; we need to evaluate whether MIBG imaging is more useful than available methods for triage of patients to transplantation or medical therapy. We also need to define the function of cardiac neurotransmission imaging in determining the risk of sudden death in patients with viable but denervated myocardium after myocardial infarction. Finally, we need to determine the role of cardiac

neurotransmission imaging in the early detection of autonomic neuropathy in diabetes mellitus. If the role of cardiac neurotransmission imaging in control of therapy and assessment of prognosis is established, the future of cardiac nuclear medicine will be ensured and bright.

ACKNOWLEDGMENTS

Figure 1 was provided courtesy of Dr. Dominique Le Guludec; Figure 3 was provided courtesy of Dr. Renato Valdés; Figures 4, 8, and 10 were provided courtesy of Dr. Junichi Yamazaki; and Figures 5 and 7 were provided courtesy of Dr. Michael Schäfers.

REFERENCES

1. James TN. Primary and secondary cardioneuropathies and their functional significance. *J Am Coll Cardiol.* 1983;2:983–1002.
2. Myeburg RJ, Castellanos A. Cardiac arrest and sudden cardiac death. In: Braunwald E, ed. *Heart Disease*. Philadelphia, PA: Saunders; 1997:742–747.
3. Randall WC, Ardell JL. Functional anatomy of the cardiac efferent innervation. In: Kulbertus HE, Franck G, eds. *Neurocardiology*. New York, NY: Futura Publishing; 1988:3–24.
4. Zipes DP, Inoue H. Autonomic neural control of cardiac excitable properties. In: Kulbertus HE, Franck G, eds. *Neurocardiology*. New York, NY: Futura Publishing; 1988:787–796.
5. McDougall AJ, McLeod JG. Autonomic neuropathy. I. Clinical features, investigation, pathophysiology, and treatment. *J Neurol Sci.* 1996;137:79–88.
6. Dae MW, O'Connell J, Botvinick EH, et al. Scintigraphic assessment of regional cardiac innervation. *Circulation.* 1989;79:634–644.
7. Bristow M. Mechanism of action of beta-blocking agents in heart failure. *Am J Cardiol.* 1997;80:26L–40L.
8. Colucci W. The sympathetic nervous system in heart failure. In: Hosenpud JD, Greenberg BH, eds. *Congestive Heart Failure.* Philadelphia, PA: Lippincott; 2000:189–197.
9. Esler MD, Jennings GL, Korner P, et al. Assessment of human sympathetic nervous system activity from measurements of norepinephrine turnover. *Hypertension.* 1988;11:3–20.
10. Goldstein D, Eisenhofer G, Dunn B, et al. Positron emission tomographic imaging of cardiac sympathetic innervation using 6-^{18}F-fluorodopamine: initial findings in humans. *J Am Coll Cardiol.* 1993;22:1961–1971.
11. Luxen A, Perlmutter M, Bida GT, et al. Remote, semiautomated production of 6-[^{18}F]fluoro-L-dopa for human studies with PET. *Int J Rad Appl Instrum.* 1990;41:275–281.
12. Schwaiger M, Kalff V, Rosenpire K, et al. Noninvasive evaluation of sympathetic nervous system in human heart by positron emission tomography. *Circulation.* 1990;82:357–464.
13. Rosenpire KC, Haka MS, Jewett DM, et al. Synthesis and preliminary evaluation of ^{11}C-meta-hydroxyephedrine: a false neurotransmitter agent for heart neuronal imaging. *J Nucl Med.* 1990;31:1328–1334.
14. Chakraborty PK, Gildersleeve DL, Jewett DM, et al. High yield synthesis of high specific activity ^{11}C-epinephrine for routine PET studies in humans. *Nucl Med Biol.* 1993;20:939–944.
15. Münch G, Nguyen N, Nekolla S, et al. Evaluation of sympathetic nerve terminals with ^{11}C-epinephrine and ^{11}C-hydroxyephedrine and positron emission tomography. *Circulation.* 2000;101:516–523.
16. Ungerer M, Hartmann F, Karoglan M, et al. Regional in vivo and in vitro characterization of autonomic innervation in cardiomyopathic human heart. *Circulation.* 1998;97:174–180.
17. Short JH, Darby TD. Sympathetic nervous system blocking agents: derivatives of benzylguanidine. *J Med Chem.* 1967;10:833–840.
18. Wieland DM, Brown LE, Rogers WL, et al. Myocardial imaging with a radioiodinated norepinephrine storage analog. *J Nucl Med.* 1981;22:22–31.
19. Wieland DM, Wu JI, Brown LE, et al. Radiolabeled adrenergic neuron-blocking agents: adrenomedullary imaging with ^{123}I-iodobenzylguanidine. *J Nucl Med.* 1980;21:349–353.
20. Sisson JC, Wieland DM, Sherman P, Mangner MC, Tobes MC, Jacques S. Metaiodobenzylguanidine as an index of adrenergic nervous system integrity and function. *J Nucl Med.* 1987;28:1620–1624.
21. Sisson JC, Bolgos G, Jhonson J. Measuring acute changes in adrenergic nerve activity of the heart in the living animal. *Am Heart J.* 1991;121:1119–1123.
22. Knickmeier M, Matheja P, Wichter T, et al. Clinical evaluation of no-carrier-added meta-(^{123}I)iodobenzylguanidine for myocardial scintigraphy. *Eur J Nucl Med.* 2000;3:302–307.
23. Gill JS, Hunter GJ, Gane G, Camm AJ. Heterogeneity of the human myocardial sympathetic innervation: in vivo demonstration by iodine 123-labeled metaiodobenzylguanidine scintigraphy. *Am Heart J.* 1993;126:390–398.
24. Delforge J, SyrotaA, Lancon JP. Cardiac beta-adrenergic receptor density measured in vivo using PET, CGP 12177, and a new graphical method. *J Nucl Med.* 1991;32:739–748.
25. Qing F, Rahman S, Hayes M, et al. Effect of long term β2-agonist dosing on human cardiac β-adrenoceptor expression in vivo: comparison with changes in lung and mononuclear leukocyte β-receptors. *J Nucl Cardiol.* 1997;4:532–538.
26. Schaffers M, Schober O, Lerch H, Cardia Schaffers M, Schober O, Lerch H. Cardiac sympathetic neurotransmission scintigraphy. *Eur J Nucl Med.* 1998;25;435–441.
27. Berridge MS, Nelson AD, Zheng L, et al. Specific beta-adrenergic receptor binding of carazolol measured with PET. *J Nucl Med.* 1994;35:1665–1676.
28. Visser T, vanWaarde A, van der Mark T, et al. Characterization of pulmonary and myocardial beta-adrenoceptors with S-1′-(fluorine-18)fluorocarazolol. *J Nucl Med.* 1997;38:169–174.
29. Valette H, Deleuze P, Syrota A, et al. Canine myocardial beta-adrenergic muscarinic receptor densities after denervation: a PET study. *J Nucl Med.* 1995;36:140–146.
30. Le Guludec D, Cohen A, Delforge J, et al. Increased myocardial muscarinic receptor density in idiopathic dilated cardiomyopathy: an in vivo PET study. *Circulation.* 1997;96:3416–3422.
31. Estorch M, Carrió I, Berná L, et al. Myocardial iodine-labeled metaiodobenzylguanidine uptake relates to age. *J Nucl Cardiol.* 1995;2:126–132.
32. Yamazaki J, Muto H, Ishiguro K, Okamoto H, Nakano H, Morishita T. Quantitative scintigraphic analysis of ^{123}I-MIBG by polar map in patients with dilated cardiomyopathy. *Nucl Med Commun.* 1997;3:219–229.
33. Somsen GA, Borm JJ, deMilliano PA, et al. Quantitation of myocardial iodine-123-MIBG uptake in SPECT studies: a new approach using the left ventricular cavity and a blood sample as a reference. *Eur J Nucl Med.* 1995;22:1149–1154.
34. Somsen A. *Cardiac Neuronal Dysfunction in Heart Failure Assessed by 123-Iodine Metaiodobenzylguanidine Scintigraphy* [thesis]. Amsterdam, The Netherlands: University of Amsterdam; 1996.
35. Goldstein DS, Holmes C, Cannon RE, et al. Sympathetic cardioneuropathy in dysautonomias. *N Engl J Med.* 1997;336;696–702.
36. De Marco T, Dae M, Yuen MS, et al. Iodine-123 MIBG scintigraphic assessment of the transplanted human heart: evidence for late reinnervation. *J Am Coll Cardiol.* 1995;25:927–931.
37. Schwaiger M, Hutchins GB, Kalff V. Evidence for regional catecholamine uptake and storage sites in the transplanted human heart by positron emission tomography. *J Clin Invest.* 1991;87;1681–1690.
38. Dae M, DeMarco T, Botvinick E, et al. Scintigraphic assessment of MIBG uptake in globally denervated human and canine hearts: implications and clinical studies. *J Nucl Med.* 1992;33:1444–1450.
39. Di Carli MF, Tobes MC, Mangner T, et al. Effects of cardiac sympathetic innervation on coronary blood flow. *N Engl J Med.* 1997;336:1208–1215.
40. Estorch M, Campreciós M, Flotats A, et al. Sympathetic reinnervation of cardiac allografts evaluated by ^{123}I-MIBG imaging. *J Nucl Med.* 1999;40:911–916.
41. Lerch H, Wichter T, Schamberger R, et al. Sympathetic myocardial innervation in idiopathic ventricular tachycardia and fibrillation [abstract]. *Eur J Nucl Med.* 1995;22:805.
42. Schafers M, Lerch H, Wichter T, et al. Cardiac autonomic dysfunction in patients with idiopathic ventricular tachycardia assessed by PET CGP 12177 [abstract]. *J Nucl Med.* 1997;38(suppl):171P.
43. Schafers M, Lerch H, Wichter T, et al. Cardiac sympathetic innervation in patients with idiopathic right ventricular outflow tract tachycardia. *J Am Coll Cardiol.* 1998;32:181–186.
44. Ungerer M, Bohm M, Elce J, et al. Altered expression of beta-adrenergic receptor kinase and beta-adrenergic receptors in the failing human heart. *Circulation.* 1993;87:454–463.
45. Henderson EB, Kahn JK, Corbet J, et al. Abnormal I-123-MIBG myocardial wash-out and distribution may reflect myocardial adrenergic derangement in patients with congestive cardiomyopathy. *Circulation.* 1988;78:1192–1199.
46. Merlet P, Dubois JL, Adnot S, et al. Myocardial beta-adrenergic desensitization and neuronal norepinephrine uptake function in idiopathic dilated cardiomyopathy. *J Cardiovasc Pharmacol.* 1992;19:10–16.
47. Merlet P, Valette H, Dubois JL, et al. Prognostic value of cardiac metaiodobenzylguanidine imaging in patients with heart failure. *J Nucl Med.* 1992;33:471–477.

48. Merlet P, Benvenuti C, Moyse D, et al. Prognostic value of MIBG imaging in idiopathic dilated cardiomyopathy. *J Nucl Med.* 1999;40:917–923.
49. Maunoury C, Agostini D, Acar P, et al. Impairment of cardiac neuronal function in childhood dilated cardiomyopathy: an ^{123}I-MIBG scintigraphic study. *J Nucl Med.* 2000;41:400–404.
50. Momose M, Kobayashi H, Iguchi N, et al. The comparison of parameters of I-123-MIBG scintigraphy for predicting prognosis in patients with dilated cardiomyopathies. *Nucl Med Commun.* 1999;20:529–535.
51. Cohen-Solal A, Esanu Y, Logeart D, et al. Cardiac metaiodobenzylguanidine uptake in patients with moderate chronic heart failure: relationship with peak oxygen uptake and prognosis. *J Am Coll Cardiol.* 1999;33:759–766.
52. Nakajima K, Taki J, Tonami M, et al. Decreased ^{123}I-MIBG uptake and increased clearance in various cardiac disorders. *Nucl Med Commun.* 1994;15:317–323.
53. Suwa M, Otake Y, Moriguchi A, et al. Iodine-123 metaiodobenzylguanidine myocardial scintigraphy for prediction of response to beta-blocker therapy in patients with dilated cardiomyopathy. *Am Heart J.* 1997;133:353–358.
54. Narula J, Haider N, Virmani R, et al. Programmed myocyte death in end-stage heart failure. *N Engl J Med.* 1996;335:1182–1189.
55. Fagret D, Wolf JE, Comet M. Myocardial uptake of meta-[^{123}I]-iodobenzylguanidine ([^{123}I]-MIBG) in patients with myocardial infarct. *Eur J Nucl Med.* 1989;15:624–628.
56. McGhie AI, Corbett JR, Akers MS, et al. Regional cardiac adrenergic function using I-123 meta-iodobenzylguanidine tomographic imaging after acute myocardial infarction. *Am J Cardiol.* 1991;67:236–242.
57. Nishimura T, Oka H, Sago M, et al. Serial assessment of denervated but viable myocardium following acute myocardial infarction in dogs using iodine-123 MIBG and thallium-201 chloride myocardial single photon emission tomography. *Eur J Nucl Med.* 1992;19:25–29.
58. Minardo JD, Tuli MM, Mock BH, et al. Scintigraphic and electrophysiological evidence of canine myocardial sympathetic denervation and reinnervation produced by myocardial infarction or phenol application. *Circulation.* 1988;78: 1008–1019.
59. Hartikainen J, Mäntysaari M, Kuikka J, Länsimies E, Pyörälä K. Extent of cardiac autonomic denervation in relation to angina on exercise test in patients with recent acute myocardial infarction. *Am J Cardiol.* 1994;74:760–763.
60. Hartikainen J, Kuikka J, Mantsayaari M, et al. Sympathetic reinnervation after acute myocardial infarction. *Am J Cardiol.* 1996;77:5–9.
61. Hartikainen J, Mustonen J, Kuikka J, Vanninen E, Kettunen R. Cardiac sympathetic denervation in patients with coronary artery disease without previous myocardial infarction. *Am J Cardiol.* 1997;80:273–277.
62. Nakata T, Nagao K, Tsuchihashi K, Hashimoto A, Tanaka S, Iimura O. Regional cardiac sympathetic nerve dysfunction and the diagnostic efficacy of metaiodobenzylguanidine tomography in stable coronary artery disease. *Am J Cardiol.* 1996;78:292–297.
63. Kramer CM, Nicol PD, Rogers WJ, et al. Reduced sympathetic innervation underlies adjacent noninfarcted region dysfunction during left ventricular remodelling. *J Am Coll Cardiol.* 1997;30:1079–1085.
64. Podio V, Spinnler MT, Spandonari T, et al. Regional sympathetic denervation after myocardial infarction: a follow-up study using [^{123}I]MIBG. *Q J Nucl Med.* 1995;39:40–43.
65. Matsunari I, Schricke U, Bengel FM, et al. Extent of cardiac sympathetic neuronal damage is determined by the area of ischemia in patients with acute coronary syndromes. *Circulation.* 2000;22:2579–2585.
66. Dae MW, O'Connell JW, Botvinik E, et al. Acute and chronic effects of transient myocardial ischemia on sympathetic nerve activity, density, and norepinephrine content. *Cardiovasc Res.* 1995;30:270–280.
67. Agostini D, Lecluse E, Belin A, et al. Impact of exercise rehabilitation on cardiac neuronal function in heart failure: an iodine-123 metaiodobenzylguanidine scintigraphy study. *Eur J Nucl Med.* 1998;25:235–241.
68. Estorch M, Flotats A, Serra-Grima R, et al. Influence of exercise rehabilitation on myocardial perfusion and sympathetic heart innervation in ischemic heart disease. *Eur J Nucl Med.* 2000;3:333–339.
69. Lefroy DC, DeSilva R, Choudury L, et al. Myocardial beta-adrenoceptor density is reduced in hypertrophic cardiomyopathy [abstract]. *Circulation.* 1992;86:I-26.
70. Lefroy DC, deSilva R, Choudury L, et al. Diffuse reduction of myocardial beta-adrenoceptors in hypertrophic cardiomyopathy: a study with positron emission tomography. *J Am Coll Cardiol.* 1993;22:1653–1660.
71. Schaffers M, Dutka D, Rhodes CG, et al. Myocardial pre and post-synaptic autonomic dysfunction in hypertrophic cardiomyopathy. *Circ Res.* 1998;82:56–62.
72. Li ST, Tack CJ, Fananapazir L, Goldstein DS. Myocardial perfusion and sympathetic innervation in patients with hypertrophic cardiomyopathy. *J Am Coll Cardiol.* 2000;7:1867–1873.
73. Choudury L, Guzzeti S, Lefroy DC, et al. Myocardial beta-adrenoceptors and left ventricular function in hypertrophic cardiomyopathy. *Heart.* 1996;75:50–55.
74. Lerch H, Bartenstein P, Wichter T, et al. Sympathetic innervation of the left ventricle is impaired in arrhythmogenic right ventricular disease. *Eur J Nucl Med.* 1993;20:207–212.
75. Wichter T, Hindricks G, Lerch H, et al. Regional myocardial sympathetic dysinnervation in arrhythmogenic right ventricular cardiomyopathy: an analysis using ^{123}I-MIBG scintigraphy. *Circulation.* 1994;89:667–683.
76. Wichter T, Lerch H, Schafers M, et al. Reduction of postsynaptic beta-receptor density in arrhythmogenic right ventricular dysplasia: assessment with positron emission tomography [abstract]. *Circulation.* 1996;94(suppl I):I-543.
77. Wichter T, Schafers M, Rhodes CG, et al. Abnormalities of cardiac sympathetic innervation in arrhythmogenic right ventricular cardiomyopathy: quantitative assessment of presynaptic norepinephrine reuptake and postsynaptic beta-adrenergic receptor density with PET. *Circulation.* 2000;13:1552–1558.
78. Kim SJ, Lee JD, Ryu YH, et al. Evaluation of cardiac sympathetic neuronal integrity in diabetic patients using iodine-123 MIBG. *Eur J Nucl Med.* 1996;23: 401–406.
79. Scognamiglio R, Avogaro A, Casara D, et al. Myocardial dysfunction and adrenergic cardiac innervation in patients with insulin-dependent diabetes. *J Am Coll Cardiol.* 1998;31:404–412.
80. Hattori N, Tamaki N, Hayasi T, et al. Regional abnormality of iodine-123-MIBG in diabetic hearts. *J Nucl Med.* 1996;37:1985–1990.
81. Morimoto S, Terada K, Keira N, et al. Investigation of the relationship between regression of hypertensive cardiac hypertrophy and improvement of cardiac sympathetic nervous dysfunction using iodine-123-MIBG. *Eur J Nucl Med.* 1996;23:756–761.
82. Morimitsu T, Miyahara Y, Sinboku H, et al. Iodine-123-metaiodobenzylguanidine myocardial imaging in patients with right ventricular pressure overload. *J Nucl Med.* 1996;37:1343–1346.
83. Sakamaki F, Satoh T, Nagaya N, et al. Correlation between severity of pulmonary arterial hypertension and ^{123}I-metaiodobenzylguanidine left ventricular imaging. *J Nucl Med.* 2000;7:1127–1133.
84. Wakasugi S, Fischman AJ, Babich JW, et al. Metaiodobenzylguanidine: evaluation of its potential as a tracer for monitoring doxorubicin cardiomyopathy. *J Nucl Med.* 1993;34:1282–1286.
85. Valdés Olmos RA, ten Bokkel Huinink WW, ten Hoeve RF, et al. Assessment of anthracycline-related myocardial adrenergic derangement by ^{123}I-MIBG scintigraphy. *Eur J Cancer.* 1995;31A:26–31.
86. Carrió I, Estorch M, Berná L, et al. ^{111}In-antimyosin and ^{123}I-MIBG studies in the early assessment of doxorubicin cardiotoxicity. *J Nucl Med.* 1995;36:2044–2049.
87. Münch G, Ziegler S, Nguyen BS, et al. Scintigraphic evaluation of cardiac autonomic innervation. *J Nucl Cardiol.* 1996;3:265–277.
88. Tamaki N. Imaging of cardiac neuronal and receptor function. *J Nucl Cardiol.* 1997;4:553–554.
89. Vaidyanathan G, Zhao XG, Strickland DK, Zalutsky MR. No-carrier-added iodine-131-FIBG: evaluation of an MIBG analog. *J Nucl Med.* 1997;38:330–334.
90. Hicks RJ, Kassiou M, Eu P, et al. Iodine 123 N-methyl-4-iodoexetimide: a new radioligand for single photon emission tomographic imaging of myocardial muscarinic receptors. *Eur J Nucl Med.* 1995;22:339–345.
91. Fischman A. Radionuclide imaging probes for expressed proteins. *J Nucl Cardiol.* 1999;6:438–448.
92. Takahashi T, Ido T, Ootake A, et al. ^{18}F-labeled 1,2-diacylglicerols: a new tracer for the imaging of second messenger systems. *J Labeled Radiopharm.* 1994;35: 517–519.
93. Liggett SB, Wagoner LE, Craft LL, et al. The Ile164 beta2-adrenergic receptor polymorphism adversely affects the outcome of congestive heart failure. *J Clin Invest.* 1998;102:1534–1539.

The Journal of NUCLEAR MEDICINE

Cardiac Neurotransmission Imaging*

Ignasi Carrió

J Nucl Med. 2001;42:1062-1076.

The Journal of Nuclear Medicine is published monthly.
SNMMI | Society of Nuclear Medicine and Molecular Imaging
1850 Samuel Morse Drive, Reston, VA 20190.
(Print ISSN: 0161-5505, Online ISSN: 2159-662X)

SNMMI SOCIETY OF NUCLEAR MEDICINE AND MOLECULAR IMAGING